Effect of HNO_3 and HCl on D_2O Desorption Kinetics from Crystalline D_2O Ice

Frank E. Livingston and Steven M. George*

Department of Chemistry and Biochemistry, University of Colorado, Boulder, Colorado 80309-0215

Received: June 15, 1998; In Final Form: October 14, 1998

The presence of trace species may perturb H_2O desorption kinetics from ice surfaces and alter the stability of atmospheric ice particles. To investigate the effects of atmospheric species on H_2O desorption kinetics from crystalline ice, the D_2O desorption kinetics from pure and HNO_3- and HCl-dosed crystalline D_2O ice multilayers on Ru(001) were investigated using isothermal laser-induced thermal desorption (LITD) measurements. The D_2O desorption kinetics were studied for D_2O ice film thicknesses of 25−200 BL (90−730 Å) and initial acid coverages of 0.5−3.0 BL for HNO_3 and 0.3−5.0 BL for HCl. Arrhenius analysis of the D_2O desorption rates from pure D_2O crystalline ice at $T = 150-171$ K yielded a desorption activation energy of $E_d = 13.7 \pm 0.5$ kcal/mol and a zero-order desorption preexponential of $\nu_o = (3.3 \pm 0.7) \times 10^{32}$ molecules/(cm^2 s). The absolute D_2O desorption rates were ∼3−5 times smaller for D_2O ice films exposed to HNO_3. The D_2O desorption kinetics from HNO_3-dosed ice were $E_d = 11.3 \pm 0.4$ kcal/mol and $\nu_o = (5.0 \pm 0.9) \times 10^{28}$ molecules/(cm^2 s). In contrast, the absolute D_2O desorption rates were ∼2 times larger for D_2O ice films exposed to HCl. The D_2O desorption kinetics from HCl-dosed ice were $E_d = 14.2 \pm 0.6$ kcal/mol and $\nu_o = (3.7 \pm 0.8) \times 10^{33}$ molecules/(cm^2 s). The changes in the D_2O isothermal desorption kinetics were independent of DNO_3 and DCl coverages. The adsorbate-induced perturbations are believed to be associated with the formation of stable hydrate cages and reduced D_2O mobility in HNO_3-dosed ice and the creation of defects and enhanced D_2O mobility in HCl-dosed ice. The effects of HNO_3 and HCl on the D_2O desorption kinetics indicate that the growth, stability, and lifetimes of atmospheric ice particles should be altered by the presence of adsorbates on the ice surface.

I. Introduction

Ice surfaces are prevalent in nature and play a special role in global atmospheric and environmental chemistry,[1−5] as well as cometary and interstellar chemistry.[6−12] Particular attention has been focused on the role of ice particles in the heterogeneous chemistry of the Antarctic polar stratosphere[1−5,13−18] and upper troposphere.[19−25] For example, polar stratospheric cloud (PSC) particles are an important component in the seasonal depletion of ozone in the Antarctic.[1,2,4,5,13,16−18] Stratospheric ice particles, composed of either concentrated solutions of nitric acid (type I PSC) or water−ice (type II PSC) convert stable forms of reservoir chlorine into photochemically labile chlorine species by heterogeneous reactions such as $ClONO_2 + HCl \rightarrow Cl_2 + HNO_3$. The active chlorine molecules can then be photolyzed to produce Cl radicals that can catalytically destroy ozone.

Chemical and physical processes on cirrus ice clouds can also have a direct and dramatic impact on tropospheric chemistry.[19,20,23−25] Recent experimental measurements[26−30] and modeling simulations[19] have been combined to show that heterogeneous chlorine activation on cirrus clouds could severely affect the chlorine and ozone levels in the tropopause region. In particular, these modeling studies have revealed that heterogeneous reactions involving $ClONO_2$, HCl, and HOCl on cirrus ice particles occur rapidly and can markedly affect NO_x and ClO_x chemistry in the upper troposphere.[19]

Subvisible cirrus clouds located predominantly near the tropical tropopause can also significantly affect the Earth's climate and the global radiation budget.[20,23−25] Thin highly reflective cirrus ice particles can alter climate feedback loops by the efficient absorption of longwave infrared radiation and emission at the low temperatures of the tropical tropopause.[20,25] These radiative effects may perturb circulation in the lower stratosphere[31] and cause dehydration of stratospheric air via freeze-drying and radiative destabilization of high altitude anvils.[32,33]

Optical interference techniques[34,35] and laser-induced thermal desorption (LITD) probing and desorption depth-profiling methods[36−40] have been employed recently to study adsorption, desorption, and diffusion processes on single-crystal ice. The optical interference measurements[34,35] have demonstrated that the ice surface is in rapid dynamic flux with H_2O molecules desorbing from the ice at rates of approximately 1×10^{16} to 1×10^{18} molecules/(cm^2 s) or ∼10−1100 BL/s at typical polar stratospheric temperatures from 180 to 210 K. The LITD diffusion measurements[36−40] have further revealed that H_2O molecules readily diffuse into the pure crystalline ice bulk on the microsecond to millisecond time scale at stratospheric temperatures. The dynamic nature of the ice surface may influence the kinetics and mechanisms of the important heterogeneous reactions on PSCs and cirrus ice clouds.[34,41] The formation, growth, and stability of ice particles in the troposphere and stratosphere will also be dependent on these H_2O adsorption, desorption, and diffusion kinetics.

Many previous investigations have studied H_2O desorption from crystalline and amorphous ice.[36−39,42−46] Recent studies have confirmed that H_2O desorption from crystalline ice follows zero-order desorption behavior.[39] The zero-order isothermal desorption rate is constant versus time and consistent with the linear removal of H_2O from the crystalline ice multilayer. In

* Corresponding author: fax, 303-492-5894; e-mail: georges@spot.colorado.edu.

10.1021/jp982627y CCC: $15.00
Published on Web 11/20/1998

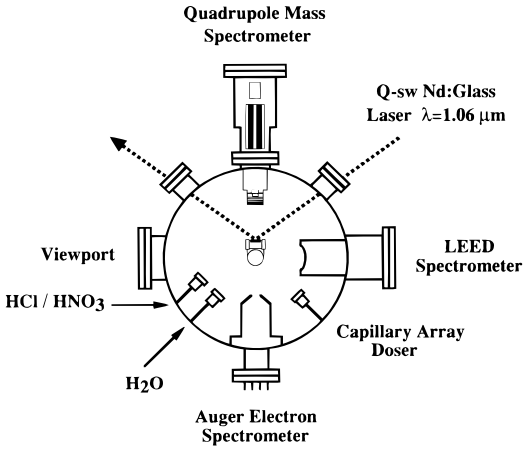

Figure 1. Schematic representation of the laser-induced thermal desorption (LITD) experimental apparatus.

contrast, only limited work has focused on the effects of surface-adsorbed species on the vaporization kinetics of crystalline ice.[44,47−49]

The presence of trace tropospheric and stratospheric species, such as HNO_3 and HCl, may perturb the adsorption, desorption, and diffusion kinetics of H_2O on crystalline ice. Early work investigated the effects of various impurities and observed that the ionic impurities generally decreased the overall vaporization rates of the ice crystals.[44] A recent study of the effect of HCl, HNO_3, and SO_2 also concluded that these gases reduce the H_2O evaporation rate from ice.[49] In addition, computer modeling studies have explored the effects of trace solutes and have determined that solute impurities significantly retard the evaporation rate of ice crystals.[50,51]

To investigate the effects of trace atmospheric species on the dynamic nature of ice, the present study measured the D_2O desorption kinetics from pure and HNO_3- and HCl-dosed single-crystal D_2O ice multilayers. The crystalline D_2O ice films were grown epitaxially on a single-crystal Ru(001) metal substrate. Measurements of the D_2O desorption kinetics were accomplished using laser-induced thermal desorption (LITD) probing.[36−38,46] The LITD experiments permitted the D_2O coverage to be monitored in real time during isothermal multilayer desorption. The temperature dependence of the desorption rates yielded the activation energies and preexponentials for D_2O desorption from pure and HNO_3- and HCl-dosed ice multilayers. These D_2O desorption kinetics were also employed to estimate the D_2O vapor pressure of pure and HNO_3- and HCl-dosed crystalline D_2O ice and to determine the effect of HNO_3 and HCl on the stability of atmospheric ice particles.

II. Experimental Section

A. Laser-Induced Thermal Desorption (LITD) Experimental Apparatus. The LITD experimental apparatus employed in the isothermal desorption measurements is shown in Figure 1.[52] Briefly, the LITD measurements were performed in an ultrahigh vacuum (UHV) chamber pumped by ion and titanium sublimation pumps. Typical background pressures in the UHV apparatus were less than 2×10^{-10} Torr. A single-crystal Ru(001) metal substrate ~1 cm in diameter was used to grow crystalline D_2O ice multilayers. Trace elemental C, S, and O contaminants were removed from the Ru(001) surface using standard cleaning procedures.[53] The ice film surface structure and surface cleanliness of the Ru(001) metal substrate were verified using low-energy electron diffraction (LEED) and Auger electron spectroscopy (AES) with a single-pass cylindrical mirror analyzer.

The desorption experiments were performed by monitoring the D_2O coverage on the Ru(001) substrate during isothermal desorption. A TEM-00 Q-switched Nd:phosphate glass laser was used to desorb thermally the ultrathin crystalline ice film. The Q-switched Nd:phosphate glass laser has an output wavelength of $\lambda = 1.06$ μm and typical pulselengths of ~100 ns. Laser pulses with energies of ~0.20 mJ/pulse were focused onto the Ru(001) substrate at an incident angle of 54° with respect to the surface normal. This optical geometry produced elliptical desorption areas with typical dimensions of ~150 μm × ~250 μm as measured by spatial autocorrelation methods.[54]

The crystalline D_2O ice film is transparent to the $\lambda = 1.06$ μm infrared radiation.[55] The incident Nd:phosphate glass laser energy is absorbed efficiently by the underlying Ru(001) metal substrate.[56] The illuminated surface area experiences a rapid temperature transient and the molecules in the column region above the focused laser beam are thermally desorbed. The desorbed species are mass analyzed with high sensitivity using an Extrel C50 quadrupole mass spectrometer with line-of-sight to the ionizer.

B. Growth of Crystalline Ice Multilayers. To study H_2O isothermal desorption on ice that structurally resembles hexagonal ice particles present in the troposphere and stratosphere, single-crystal ice multilayers were grown epitaxially on a single-crystal Ru(001) metal substrate. The single-crystal Ru(001) metal has an excellent lattice match to the geometry of naturally occurring hexagonal ice. The lattice constant of the $\sqrt{3}\times\sqrt{3}$R30° unit cell on Ru(001) is 4.68 Å[57] which closely matches the nearest-neighbor oxygen−oxygen distance of 4.50 Å in the first bilayer on the basal plane of I_h ice.[58] The close lattice match facilitates the epitaxial growth of highly ordered crystalline ice multilayers with minimal distortion (<4%) of the hexagonal ice lattice.

Gaseous isotopically labeled water (D_2O, ≥99.996% ^2H, Cambridge Isotope Laboratories) was adsorbed on the Ru(001) substrate using a glass multichannel capillary array doser. The crystalline D_2O ice multilayers were grown by either capillary array D_2O vapor deposition at 160 K or by dosing D_2O at 120 K followed by multilayer annealing at 160 K.[37,38] Previous LEED measurements on H_2O ice multilayers have confirmed that both methods of ice multilayer preparation yield well ordered hexagonal ice films.[36]

C. Measurement of Isothermal Desorption by LITD. Measurements of D_2O desorption from pure and HNO_3- and HCl-dosed crystalline D_2O ice films were performed by LITD monitoring of the D_2O coverage (Θ) in real time during isothermal desorption. A crystalline D_2O ice multilayer was initially grown on the Ru(001) substrate. LITD analysis of the crystalline ice multilayer was conducted prior to adsorbate exposure to check for the adsorption of background H_2O and HDO impurities. LITD analysis confirmed that the D_2O ice films were pure with a typical initial HDO impurity content of ≤0.7%.

The D_2O ice multilayer was then exposed to either nitric acid (HNO_3) or hydrogen chloride (HCl) at 120 K using a separate capillary array doser. Rapid H/D isotopic exchange at the multilayer surface resulted in the formation of a HDO adlayer along with a stoichiometric quantity of DNO_3 or DCl. Typical HNO_3 and HCl exposures were performed at pressures ranging from $\sim 1 \times 10^{-7}$ Torr to $\sim 1 \times 10^{-6}$ Torr for times from 10 to 30 s. Although the interaction of HNO_3 and HCl with ice may eventually lead to the formation of macroscopic stable HNO_3−hydrate[48,59−65] and HCl−hydrate[47,62,66−69] phases, formation of these hydrates is unlikely given the small HNO_3 and HCl

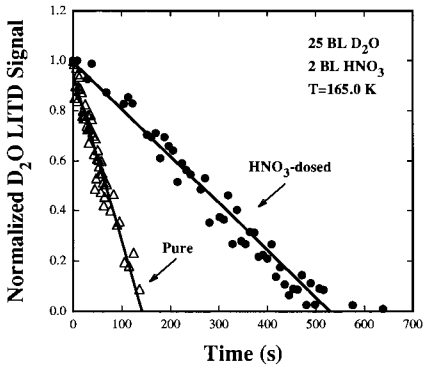

Figure 2. Normalized D_2O LITD signals versus time for isothermal desorption at $T = 165.0$ K of a pure 25 BL D_2O ice multilayer and a 25 BL D_2O ice multilayer dosed with 2 BL of HNO_3. The D_2O LITD signals for the pure ice film and the HNO_3-dosed ice film are represented by the open triangles and solid circles, respectively.

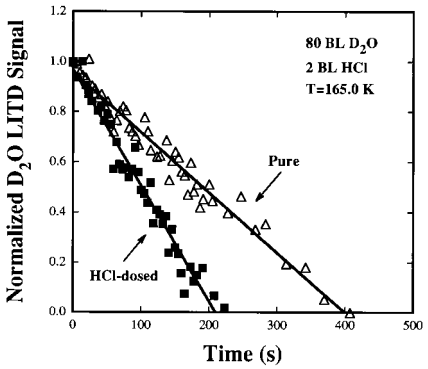

Figure 3. Normalized D_2O LITD signals versus time for isothermal desorption at $T = 165.0$ K of a pure 80 BL D_2O ice multilayer and a 80 BL D_2O ice multilayer dosed with 2 BL of HCl. The D_2O LITD signal for the pure ice film and the HCl-dosed ice film are represented by the open triangles and solid squares, respectively.

exposures. The initial acid adlayer coverages were quantified by the HDO LITD signals resulting from H/D isotopic exchange.[37,38,40] The acid coverages were low and ranged from only 0.5−3.0 BL for HNO_3 and 0.3−5.0 BL for HCl.

Initially, the crystalline ice temperature was maintained below 90 K using a liquid nitrogen cooled cryostat in direct thermal contact with the Ru(001) crystal. This low temperature prevents any thermal desorption of the ice film. The annealed crystalline D_2O ice multilayers were then resistively heated from <90 K to the desired desorption temperature at a rate of ∼1 K/s. The ice crystal temperature was maintained at the desorption temperature and the D_2O coverage was measured by LITD probing in real time during isothermal desorption. For the LITD measurements, the laser beam was translated across the ice multilayer using mirrors mounted on piezoelectric translators equipped with optical encoders. The laser pulses interrogated the surface coverages at different spatial locations at different times. The D_2O coverages were monitored until the crystalline ice multilayer was completely desorbed from the Ru(001) substrate.

The HNO_3 vapor was extracted from a mixture of commercial nitric acid (HNO_3, Mallinckrodt, 69.4 wt %) and sulfuric acid (H_2SO_4, Mallinckrodt, 96.1 wt %) in a 1:3 volume ratio. The H_2SO_4 effectively removes trace water impurity from the source HNO_3.[70] The resulting vapor over the HNO_3/H_2SO_4 mixture is >95% HNO_3 by mass and contains only a small contribution from H_2O impurity.[70] The HNO_3/H_2SO_4 mixture was purified by several freeze−pump−thaw cycles with liquid nitrogen prior to use. Gaseous HCl was obtained from Aldrich Chemical Co., Inc. (HCl, >99% anhydrous grade) and used without further purification.

III. Results

A. Desorption of Pure and HNO_3-Dosed Crystalline Ice Multilayers. Figure 2 shows a comparison between the isothermal desorption of a pure D_2O ice multilayer and a D_2O ice multilayer that was exposed to HNO_3 prior to desorption at $T = 165.0$ K. The initial D_2O coverage for the pure and HNO_3-dosed ice films was 25 BL as measured by LITD probing prior to isothermal desorption. The normalized D_2O LITD signals for the pure ice film and HNO_3-dosed ice film are represented by open triangles and solid circles, respectively. The solid lines represent linear least-squares fits to the D_2O isothermal desorption data. The initial HNO_3 adlayer coverage was 2 BL for the HNO_3-dosed ice multilayer. One bilayer (BL) is defined as 1.06×10^{15} molecules/cm^2 and corresponds to the number of H_2O molecules in the $\sqrt{3}\times\sqrt{3}$R30° ice-like bilayer on Ru(001).[71]

The D_2O LITD signal for the 25 BL pure D_2O ice multilayer in Figure 2 decreases linearly versus time until the ice film is completely desorbed after ∼140 s. The loss of D_2O versus time is consistent with zero-order desorption kinetics and linear D_2O removal with no significant changes in ice film surface area during isothermal desorption.[39] The slightly nonuniform D_2O spatial coverage distribution resulting from the multichannel capillary array doser introduces a scatter on the individual LITD signals of less than ±10%.[39] The measured isothermal desorption rate for the pure D_2O ice film at $T = 165.0$ K is $\sim 1.9 \times 10^{14}$ molecules/(cm^2 s) or ∼0.2 BL/s and remains constant for ice multilayer thicknesses ranging from 25 to 200 BL D_2O. This LITD isothermal desorption data is in excellent agreement with the D_2O desorption kinetics measured previously using LITD spatial measurements and isothermal desorption flux analysis.[39]

In comparison, the 25 BL D_2O ice film that was exposed to HNO_3 required approximately 525 s to desorb completely from the Ru(001) substrate. The desorption flux for the HNO_3-dosed D_2O ice multilayers was measured to be $\sim 5.1 \times 10^{13}$ molecules/(cm^2 s) or ∼0.05 BL/s. The isothermal desorption results in Figure 2 clearly reveal that the presence of HNO_3 on the ice multilayer surface markedly decreases the D_2O desorption rate by a factor of ∼4 at $T = 165.0$ K. Similar reductions by factors by ∼3−5 in the isothermal D_2O desorption rate were obtained for HNO_3-dosed crystalline ice multilayers for temperatures from 150 to 171 K. For these measurements, the D_2O ice multilayers ranged in thickness from 25 to 200 BL and HNO_3 coverages varied from 0.5 to 3.0 BL.

B. Desorption of Pure and HCl-Dosed Crystalline Ice Multilayers. LITD techniques were also used to monitor the effect of HCl on the D_2O isothermal desorption rate from crystalline D_2O ice multilayers. The normalized D_2O LITD signals versus time for the isothermal desorption of a pure D_2O ice film and a HCl-dosed D_2O ice film at $T = 165.0$ K are shown together in Figure 3. The initial D_2O coverages were 80 BL and the HCl adlayer thickness was 2 BL as measured by LITD probing prior to isothermal desorption. The D_2O LITD signals for the pure D_2O ice multilayer and the HCl-dosed D_2O ice multilayer are denoted by the open triangles and solid squares, respectively.

The normalized D_2O LITD signal for the pure ice film again decays linearly versus time and is consistent with zero-order desorption kinetics. The LITD results show that the 80 BL pure D_2O ice multilayer is thermally desorbed in ∼400 s and

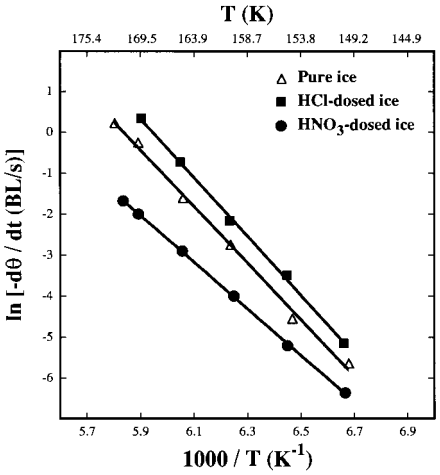

Figure 4. Arrhenius plot of D_2O desorption rates from crystalline D_2O ice multilayers. The desorption kinetic parameters for pure ice are $E_d = 13.7$ kcal/mol and $\nu_o = 3.3 \times 10^{32}$ molecules/(cm^2 s). The desorption kinetic parameters for HNO_3-dosed ice are $E_d = 11.3$ kcal/mol and $\nu_o = 5.0 \times 10^{28}$ molecules/(cm^2 s). The desorption kinetic parameters for HCl-dosed ice are $E_d = 14.2$ kcal/mol and $\nu_o = 3.7 \times 10^{33}$ molecules/(cm^2 s).

corresponds to a desorption rate of $\sim 2.1 \times 10^{14}$ molecules/(cm^2 s) or ~ 0.2 BL/s at $T = 165.0$ K. In contrast, the 80 BL D_2O ice multilayer exposed to HCl desorbs appreciably faster compared with the pure D_2O ice film. The 80 BL D_2O ice film with a 2 BL HCl adlayer required only ~ 210 s to desorb completely. This result corresponds to a desorption rate of $\sim 4.0 \times 10^{14}$ molecules/(cm^2 s) or ~ 0.4 BL/s.

In contrast to the HNO_3-dosed ice multilayers, Figure 3 clearly demonstrates that the isothermal D_2O desorption rate is enhanced by a factor ~ 2 in the presence of HCl at $T = 165.0$ K. This desorption rate enhancement was measured for HCl-dosed D_2O ice multilayers for temperatures from 150 to 170 K. For these measurements, the ice multilayers ranged in thickness from 25 to 200 BL of D_2O and initial HCl coverages varied from 0.3 to 5.0 BL of HCl.

C. Arrhenius Analysis of D_2O Desorption. The temperature dependence of the D_2O desorption rates for pure and HNO_3- and HCl-dosed crystalline ice multilayers were investigated to extract the desorption kinetics parameters. Arrhenius plots of the measured D_2O desorption rates are shown in Figure 4. The desorption results for the pure and HNO_3- and HCl-dosed ice multilayers are represented by the open triangles, solid circles, and solid squares, respectively. The solid lines represent least-squares linear regressions of the Arrhenius desorption data.

Arrhenius analysis of the D_2O desorption rates yielded the desorption activation energies and desorption preexponentials. For pure D_2O ice multilayers, the kinetic parameters were $E_d = 13.7 \pm 0.5$ kcal/mol and $\nu_o = (3.3 \pm 0.7) \times 10^{32}$ molecules/(cm^2 s). For HNO_3-dosed ice films, the kinetic parameters were $E_d = 11.3 \pm 0.4$ kcal/mol and $\nu_o = (5.0 \pm 0.9) \times 10^{28}$ molecules/(cm^2 s). The kinetic parameters for D_2O desorption from HCl-dosed ice multilayers were $E_d = 14.2 \pm 0.6$ kcal/mol and $\nu_o = (3.7 \pm 0.8) \times 10^{33}$ molecules/(cm^2 s).

D. Isothermal Desorption of DNO_3 and DCl from Crystalline Ice Multilayers. The isothermal desorption of DNO_3 and DCl from the crystalline ice multilayer can also be monitored using LITD probing. Figure 5 shows a comparison between the D_2O and DNO_3 LITD signals during isothermal desorption at 160.0 K for a D_2O ice multilayer with an initial coverage of 40 BL. The initial coverage of DNO_3 was 2.8 BL as measured by the HDO LITD signal resulting from H/D isotopic exchange

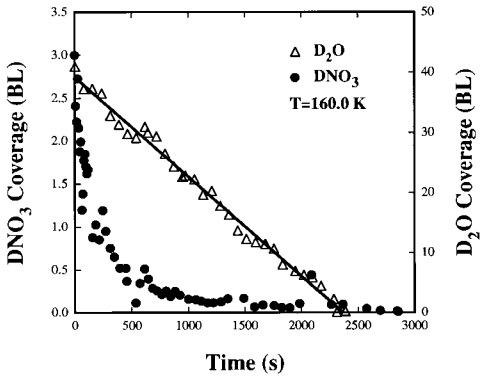

Figure 5. DNO_3 and D_2O coverages versus time for isothermal desorption at 160.0 K of a 40 BL D_2O ice multilayer with ~ 3 BL of HNO_3. The DNO_3 and D_2O LITD signals are denoted by the solid circles and open triangles, respectively.

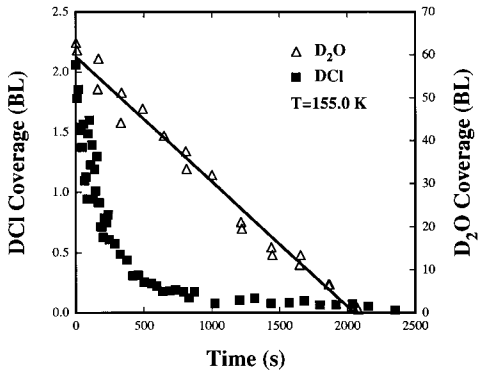

Figure 6. DCl and D_2O coverages versus time for isothermal desorption at 155.0 K of a 62 BL D_2O ice multilayer with ~ 2 BL of HCl. The DCl and D_2O LITD signals are denoted by the solid squares and open triangles, respectively.

after HNO_3 exposure. The D_2O LITD signals are shown by the open triangles. The DNO_3 LITD signals are displayed by the solid circles.

Figure 5 reveals that D_2O is lost linearly versus time from the HNO_3-dosed D_2O multilayer in agreement with zero-order desorption kinetics. Notice that the D_2O desorption rate is not sensitive to the absolute DNO_3 coverage. Figure 5 shows that the D_2O multilayer is desorbed at a constant rate for DNO_3 coverages varying from 3.0 to 0.1 BL. In contrast, the DNO_3 LITD signals do not display a linear loss versus time. The absolute initial DNO_3 desorption rate of ~ 0.01 BL/s is less than the absolute D_2O desorption rate of ~ 0.02 BL/s at 160.0 K. The nonlinear desorption behavior for DNO_3 is attributed to the competition between DNO_3 isothermal desorption and DNO_3 diffusion into the underlying ice film.[37,38,40,41,72]

Figure 6 compares the D_2O and DCl LITD signals during isothermal desorption at 155.0 K for a D_2O ice multilayer with an initial coverage of 62 BL. The initial coverage of DCl was 2.2 BL as measured by the HDO LITD signal resulting from H/D isotopic exchange after HCl exposure. The D_2O LITD signals are designated by the open triangles and the DCl LITD signals are shown by the solid squares.

Figure 6 shows that D_2O loss is linear versus time from the HCl-dosed D_2O multilayer as expected from zero-order desorption kinetics. Like the previous measurements for DNO_3, the D_2O desorption rate is not dependent on the absolute DCl coverage. The D_2O multilayer is desorbed at a constant rate for DCl coverages that range from 2.2 to 0.1 BL. The DCl LITD signals do not display a linear loss versus time. The absolute initial desorption rate of $\sim 6.0 \times 10^{-3}$ BL/s for DCl is less than

the absolute desorption rate of ~0.03 BL/s for D_2O at 155.0 K. Similar to DNO_3, the nonlinear loss of DCl is assigned to the concurrent DCl isothermal desorption and DCl diffusion into the underlying ice multilayer.[37,38,40,41,72]

IV. Discussion

A. Effect of DNO_3 and DCl on D_2O Isothermal Desorption Kinetics. The D_2O desorption kinetics from crystalline D_2O ice multilayers on Ru(001) were altered significantly upon exposure to HNO_3 and HCl. The absolute D_2O desorption rates from HNO_3-dosed crystalline ice were ~3−5 times slower compared with D_2O desorption from pure D_2O ice films over the temperature range $T = 150-171$ K. In contrast, the absolute D_2O desorption rates were ~2 times faster for crystalline ice films exposed to HCl.

Although the effect of solutes on the evaporation rate of liquid H_2O has been examined extensively,[73−77] limited work exists with regard to the effects of adsorbates on the desorption of H_2O ice.[44,47−49] Recent cold chamber experiments have examined the uptake of several atmospheric trace gases on ice and the effects of these gases on the evaporation rate of macroscopic (4−10 mm diameter) ice hemispheres and dendritic ice crystals.[49] These evaporation studies measured the mass loss versus time from ice particles that had been exposed to HNO_3, SO_2, and mixtures of SO_2 and H_2O_2. Ice crystals containing HNO_3 and SO_2 impurities were observed to evaporate isothermally up to 30% slower compared with the evaporation rate of pure ice particles at $T = 254$ K.[49]

Vacuum microbalance techniques have been utilized to study the influence of various lattice and surface-localized impurities on the vaporization rate of ice single crystals.[44] These vaporization studies measured the H_2O desorption rate from crystalline ice doped with monovalent species such as HF, HNO_3, NH_4OH, and NaOH. Ice doped with ionic impurities was observed to desorb at steady-state rates that were slower compared with pure crystalline ice at temperatures from $T = 183-233$ K.[44]

The influence of a variety of gases was also investigated using the microbalance techniques.[44] H_2, He, N_2, O_2, and CO_2 were found to decrease slightly the H_2O desorption rate from single-crystal ice. In these studies, the impurity gas flux incident on the ice surface and the ice vaporization flux were of similar magnitude. The observed decrease in the desorption rate was attributed to gas-phase collisions occurring near the vaporizing ice surface.[44] In contrast, the presence of HF on the ice surface was measured to increase the H_2O desorption rate from single-crystal ice.[44] The desorption rate of ice exposed to HF was ~1.6 times faster than the desorption rate of pure crystalline ice at $T = 214$ K.

Incorporation of HF into the ice lattice is believed to occur in a substitutional manner.[78−80] Due to the proton deficiency of the HF molecule, lattice substitution results in the formation of a L-type (L = Leer or empty) Bjerrum defect.[78−80] The generation of a Bjerrum orientational L-defect will produce a pair of neighboring O-atoms without an intervening H-atom. The HF-induced orientational Bjerrum defects can act to rupture the ordered hydrogen bonding network on the ice surface and alter H_2O desorption rates. Further evidence of HF-induced defect formation and disruption of the surface hydrogen bonding network is corroborated by the observed softening of ice by HF.[81,82]

Similar to HF, substitutional incorporation of HCl into the ice lattice is expected and has been inferred from dielectric relaxation measurements[83] on HCl-doped ice and molecular dynamics simulations[84] of HCl ionization on ice. The formation of L-defects by HCl or its ionization products may disrupt and weaken the hydrogen bonds in the top layers on the ice multilayer and enhance the H_2O desorption rates. Perturbations of the ice by HCl and the formation of L-defects are further corroborated by measurements of HCl-induced ice softening.[85]

H_2O desorption is also believed to be rate-limited by the population of highly mobile H_2O precursor molecules that are hydrogen-bonded to only one nearest neighbor.[44] The production of these highly mobile H_2O molecules may be altered by surface impurities that affect the hydrogen bonding network on the ice surface. Recent LITD diffusion experiments have revealed that HDO diffusion in HCl-dosed D_2O ice multilayers occurs ~10−20 times faster compared with HDO diffusion in pure D_2O crystalline ice for temperatures from 146 to 161 K.[40,72] This enhanced mobility may increase the desorption rate by allowing the population of the highly mobile H_2O precursors to H_2O desorption to be replenished at a faster rate.

If H_2O desorption is rate-limited by the production of highly mobile H_2O precursors, the kinetics for H_2O diffusion may directly affect the H_2O desorption kinetics. Previous LITD studies of HDO diffusion in ice exposed to HCl measured a HDO diffusion activation energy of $E_A = 19.0 \pm 0.3$ kcal/mol and a diffusion preexponential of $D_o = (2.4 \pm 0.1) \times 10^{12}$ cm^2/s for temperatures $T = 146-161$ K.[40,72] These HDO diffusion parameters in HCl-dosed ice are larger than the kinetic parameters of $E_A = 17.0 \pm 1.0$ kcal/mol and $D_o = (4.2 \pm 0.8) \times 10^8$ cm^2/s measured for pure ice.[37,38,72] In accord with a diffusion-limited desorption process, the larger kinetic parameters for D_2O desorption from HCl-dosed ice may reflect the larger diffusion activation barrier and diffusion preexponential for D_2O diffusion in HCl-dosed ice.

In contrast to the results for HCl-dosed ice, the D_2O desorption rates from HNO_3-dosed ice multilayers were measured to be lower than the D_2O desorption rates from pure ice. The different effect of HNO_3 on D_2O desorption suggests that a different mechanism is applicable. Instead of substitutional incorporation and an increase in ice lattice defect density, HNO_3 can ionize and form stable hydrate cages with H_2O.[86] For example, X-ray crystallography[87] and ab initio quantum mechanical studies[86] on solid nitric acid monohydrate (NAM) are consistent with a crystal structure comprised of NO_3^- and H_3O^+ ions. In the orthorhombic NAM crystal lattice, the nitrate and hydronium ions are bound by Coulomb forces.[86] Each NO_3^- ion is hydrogen bonded to three neighboring H_3O^+ ions.[86]

The reduced D_2O desorption rate from HNO_3-dosed ice multilayers may be partly attributable to the increased stability of the nitric acid−hydrate cages. The strong Coulomb and hydrogen bond interactions in the hydrate cage structure may act to bind H_2O molecules and limit their desorption. FTIR results are consistent with the enhanced stability of H_2O:HNO_3 hydrates.[48] These FTIR studies showed that HNO_3 adsorption on pure ice in the form of nitric acid trihydrate (NAT) and nitric acid monohydrate (NAM), or a combination of NAT/NAM, inhibited the evaporation of the underlying ice film.[48]

HNO_3 exposure to crystalline ice also reduces the mobility of H_2O molecules in ice. Evidence for decreased H_2O mobility in HNO_3-dosed ice is provided by recent LITD measurements.[40,72] These LITD investigations revealed that the presence of HNO_3 decreased the HDO diffusion rate by a factor of ~30−70 compared with HDO diffusion in pure D_2O ice over the temperature range from $T = 150$ K to $T = 173$ K.[40,72] The reduced H_2O mobility in HNO_3-dosed ice may decrease the H_2O desorption by lowering the concentration of highly mobile H_2O precursors to H_2O desorption.

On the basis of a diffusion-limited desorption mechanism, the H_2O diffusion kinetics may directly influence the H_2O desorption kinetics. LITD measurements of HDO diffusion in HNO_3-dosed ice revealed that the HDO diffusion kinetic parameters are appreciably reduced compared with the HDO diffusion kinetic parameters in pure ice.[40,72] Temperature-dependent LITD experiments measured an activation energy of $E_A = 13.2 \pm 1.4$ kcal/mol and a preexponential of $D_o = 71.9 \pm 9.2$ cm^2/s for HDO diffusion in HNO_3-dosed ice over the temperature range $T = 150-173$ K.[40,72] The smaller kinetic parameters for HDO diffusion in HNO_3-dosed ice may yield the smaller activation energy and preexponential for D_2O desorption from HNO_3-dosed ice.

B. Coverage-Independent Effect of DNO_3 and DCl on D_2O Desorption. The isothermal LITD results shown in Figures 5 and 6 demonstrate that the D_2O desorption rates from HNO_3- and HCl-dosed D_2O ice multilayers are independent of the absolute DNO_3 and DCl coverage. The LITD data presented in Figure 5 reveal that only small DNO_3 coverages are necessary to decrease the D_2O isothermal desorption rate. The D_2O desorption rate is independent of the absolute DNO_3 coverage and the isothermal D_2O desorption rate remains constant at $\sim$0.02 BL/s for DNO_3 coverages varying from 0.1 to 3.0 BL.

The isothermal desorption data in Figure 6 also indicates that only the presence of small DCl coverages are required to enhance the D_2O desorption rate. The D_2O desorption rate is independent of the absolute DCl coverage and the isothermal D_2O desorption rate remains constant at $\sim$0.03 BL/s for DCl coverages varying from 0.1 to 2.2 BL. The lack of coverage dependence suggests that only a minimum DNO_3 and DCl coverage is required to perturb the D_2O ice surface and alter the D_2O desorption kinetics.

The small DNO_3 and DCl coverages of $\geq$0.1 BL needed to affect the D_2O desorption kinetics are probably related to the ability of HNO_3 and HCl to disrupt the hydrogen bonding network on the ice surface. HCl may enter the ice lattice substitutionally upon dissolution[78-80] or ionize at the ice surface.[67,84,88-90] Each Cl^- ion could directly perturb at least four H_2O molecules in the ice lattice.[84] The computer simulations also show that both trigonal and tetrahedral solvation of the H_3O^+ by H_2O are energetically favorable.[84] Given the high directionality of hydrogen bonding, small coverages of Cl^- and H_3O^+ could significantly perturb the entire hydrogen bonding network on the ice surface and into the ice lattice. Once this hydrogen bonding network is disrupted, additional HCl may not further change the surface configurations.

Ab initio quantum mechanical studies have shown that HNO_3 ionizes and forms stable hydrate cages with H_2O.[86] The HNO_3-hydrate cages are typically found in the form of either nitric acid trihydrate (NAT) or nitric acid monohydrate (NAM). In crystalline NAM, each NO_3^- ion is H-bonded to three nearest-neighbor H_3O^+ ions.[86] Consequently, a HNO_3 surface coverage of $\sim$0.3 BL may be sufficient to perturb all the H_2O molecules in the topmost bilayer of the ice multilayer. The perturbations induced by the NO_3^- ions may be propagated along the ice surface and into the ice lattice. Additional HNO_3 coverage may not continue to alter the hydrogen bonding network after this network is initially disturbed by HNO_3.

C. H_2O Desorption Kinetics and Equilibrium Vapor Pressures at Atmospheric Temperatures. The Arrhenius desorption results shown in Figure 4 for pure crystalline ice and crystalline ice exposed to HNO_3 and HCl reveal the dramatic effect of surface-adsorbed impurities on the D_2O desorption kinetics. The D_2O desorption kinetics can be extrapolated to temperatures $T = 180-250$ K that are relevant in the polar stratosphere and upper troposphere. Figure 7 shows the D_2O desorption rate versus ice surface temperature $T = 150-250$ K. The D_2O desorption rates measured in this study from $T = 150$ K to $T = 171$ K are denoted by the solid lines. Extrapolated desorption rates for higher temperatures that contain stratospheric and upper tropospheric temperatures are represented by the dashed lines for $T = 172-250$ K.

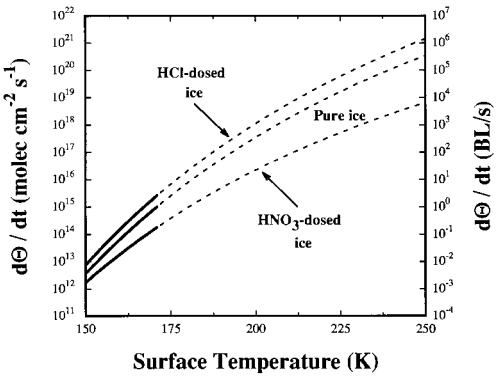

Figure 7. Desorption rate versus ice surface temperature for pure ice, ice with HNO_3 coverages $\geq$0.1 BL, and ice with HCl coverages $\geq$0.1 BL. The measured desorption rates are represented by the solid lines for $T = 150-171$ K. Extrapolated rates for higher temperatures of $T = 172-250$ K that contain stratospheric and upper tropospheric temperatures are denoted by the dashed lines.

Figure 7 shows that the presence of HNO_3 on the ice surface should appreciably decrease the D_2O desorption rates from crystalline ice by factors of $\sim$3-53. In contrast, the D_2O desorption rates from ice multilayers containing HCl should be enhanced by factors of $\sim$2-4. These changes in the D_2O desorption rates will affect the formation and stability of ice cloud particles. Changes in the stability and lifetimes of atmospheric ice crystals may subsequently alter heterogeneous atmospheric chemistry.

For example, the presence of nitric acid markedly inhibits the D_2O desorption rate from crystalline ice. This decrease in the desorption rate will increase the lifetime of ice cloud particles. HNO_3 is present in the stratosphere at partial pressures of $\sim 3 \times 10^{-7}$ Torr.[59,91] These HNO_3 partial pressures are sufficient to establish HNO_3 coverages of $\sim$2 BL in 3 s assuming a unity HNO_3 sticking coefficient and no competing HNO_3 desorption. An increased lifetime for ice cloud particles containing HNO_3 coverage will prolong the time period for heterogeneous chemical processing on PSCs and cirrus clouds. The extended lifetime of the ice crystals may also contribute to dehydration in the lower stratosphere,[32,33,92] and glaciation of lower-level clouds and storm development.[50,93,94]

The D_2O desorption kinetics can be used to calculate the equilibrium D_2O vapor pressures above pure and HNO_3- and HCl-dosed crystalline ice. To equate desorption and adsorption rates at equilibrium, these calculations assume a unity sticking coefficient on pure and HNO_3- and HCl-dosed ice. A sticking coefficient of $S \approx 1$ has been determined recently on pure crystalline ice using molecular beam and optical interference measurements.[35] Although a unity sticking coefficient is likely on HNO_3- and HCl-dosed ice, the interpretation of recent evaporation experiments suggests that HNO_3 may lower the H_2O sticking coefficient on ice.[95] Because this issue is unresolved, this analysis will proceed assuming a unity sticking coefficient.

The maximum theoretical rate of evaporation, E_{max}, of a molecule from a bulk solid is defined from gas kinetic theory as

$$E_{max} = P_v(2\pi mkT_s)^{-1/2} \quad (1)$$

Assuming a unity sticking coefficient, P_v is the vapor pressure that would be present for a system at equilibrium. Likewise, T_s is the surface temperature, m is the mass of the molecule, and k is the Boltzmann gas constant. The experimentally measured evaporation rate, E_{exp}, is related to the maximum theoretical evaporation rate by $E_{exp} = \gamma E_{max}$, where γ represents the evaporation coefficient. Measured evaporation coefficients for H_2O ice have been reported to vary from $\gamma = 0.006$ to $\gamma = 1.0$ using a variety of experimental techniques.[34,96−99] Despite the variation in the measured values for the evaporation coefficient, γ is generally assumed to be unity.[98−105]

By using $\gamma = 1.0$, E_{max} in eq 1 can be replaced by the measured zero-order desorption rate. The zero-order desorption rate at an ice surface temperature, T_s, can then be related to P_v according to

$$d\Theta/dt = \nu_o \exp[-E_d/RT_s] = P_v(2\pi mkT_s)^{-1/2} \quad (2)$$

where E_d is the desorption activation energy and ν_o is the zero-order desorption preexponential factor. Solving for P_v yields the following relation for the equilibrium vapor pressure:

$$P_v = \nu_o(2\pi mkT_s)^{1/2} \exp[-E_d/RT_s] \quad (3)$$

Figure 8 shows the calculated equilibrium water vapor pressures for pure and HNO_3- and HCl-dosed D_2O ice versus ice surface temperature at $T = 180-250$ K. The vapor pressures for pure ice were determined to vary from $P_v \approx 1.2 \times 10^{-5}$ Torr at $T = 180$ K to $P_v \approx 0.7$ Torr at $T = 250$ K. These predicted vapor pressures for pure crystalline D_2O ice are in good agreement with vapor pressure measurements for D_2O ice at temperatures $T = 193-235$ K.[106] Accounting for the different desorption rates from D_2O and H_2O ices,[46] the D_2O vapor pressures for pure D_2O ice shown in Figure 8 are also consistent with previous H_2O vapor pressure measurements.[42,43,107,108]

The suppression of the D_2O desorption rate by HNO_3 is reflected dramatically in the derived vapor pressures for ice containing HNO_3 shown in Figure 8. The vapor pressures determined from the D_2O desorption kinetics varied from $P_v \approx 1.6 \times 10^{-6}$ Torr at $T = 180$ K to $P_v \approx 0.01$ Torr at $T = 250$ K. The presence of HNO_3 on the ice surface decreases the D_2O vapor pressure by factors of ∼8−70 compared with the vapor pressures for pure ice at $T = 180-250$ K. Consequently, HNO_3 decreases the minimum H_2O pressure and/or increases the maximum temperature for PSC and cirrus cloud stability.

The vapor pressure of pure ice was determined to be $P_v \approx 6.0 \times 10^{-4}$ Torr at $T = 200$ K. For an atmospheric ice particle to be stable, equilibrium or net growth conditions must exist where the H_2O adsorption rate onto the ice particle is equal to or greater than the H_2O desorption rate. Figure 8 shows that an ice crystal with HNO_3 coverages ≥0.1 BL can increase its temperature to $T = 221$ K and still maintain a desorption rate that is less than or equal to the adsorption rate resulting from a H_2O vapor pressure of $P_v = 6.0 \times 10^{-4}$ Torr. Likewise, Figure 8 indicates that the D_2O vapor pressure for HNO_3-dosed ice at $T = 200$ K is $P_v \approx 3.8 \times 10^{-5}$ Torr. This lowering of the D_2O vapor pressure indicates that ice particles containing HNO_3 can survive at markedly smaller H_2O vapor pressures than pure ice particles.

In contrast to the results for HNO_3, the vapor pressures for ice with HCl coverages ≥0.1 BL shown in Figure 8 are much larger than pure ice. These equilibrium vapor pressures for HCl-dosed ice are ∼3−4 times higher than the vapor pressures for pure ice at temperatures $T = 180-250$ K. This increase in vapor pressure decreases the lifetime of atmospheric ice particles containing HCl. The vapor pressure for an ice film exposed to HCl was determined to be $P_v \approx 1.9 \times 10^{-3}$ Torr at $T = 200$ K. To obtain the equilibrium vapor pressure of $P_v \approx 6.0 \times 10^{-4}$ Torr for pure ice at 200 K, the temperature of the HCl-exposed ice particle must be lowered from 200 to 194 K. Alternatively, the H_2O vapor pressure must be increased to $P_v \approx 1.9 \times 10^{-3}$ Torr at $T = 200$ K to maintain an equivalence between the adsorption and desorption rates.

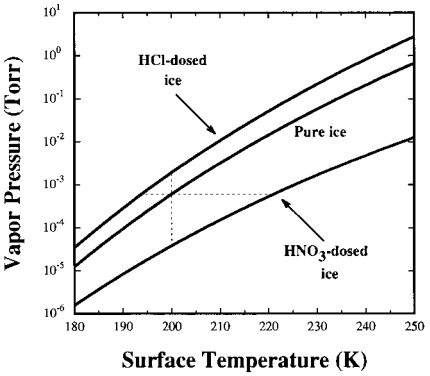

Figure 8. Equilibrium vapor pressure versus ice surface temperature for pure ice, ice with HNO_3 coverages ≥0.1 BL, and ice with HCl coverages ≥0.1 BL at temperatures of $T = 180-250$ K that are relevant in the stratosphere and upper troposphere.

V. Conclusions

The absolute D_2O desorption rates from pure and HNO_3- and HCl-dosed crystalline D_2O ice multilayers on Ru(001) were measured using laser-induced thermal desorption (LITD) techniques. The presence of the acid impurities has a dramatic impact on the D_2O desorption rates. HNO_3 coverages ≥0.1 BL lowered the D_2O desorption rate by a factor of ∼3−5 over the temperature range $T = 150-171$ K. Arrhenius analysis of the D_2O desorption rates from D_2O ice containing HNO_3 yielded a desorption activation energy of $E_d = 11.3 \pm 0.4$ kcal/mol and a zero-order desorption preexponential of $\nu_o = (5.0 \pm 0.9) \times 10^{28}$ molecules/(cm^2 s). For D_2O ice multilayers with HCl coverages >0.1 BL, the absolute D_2O desorption rates were enhanced by a factor of ∼2 for $T = 150-170$ K. The D_2O desorption kinetics from D_2O ice containing HCl were $E_d = 14.2 \pm 0.6$ kcal/mol and $\nu_o = (3.7 \pm 0.8) \times 10^{33}$ molecules/(cm^2 s). For comparison, the desorption parameters for D_2O desorption from pure D_2O ice were $E_d = 13.7 \pm 0.5$ kcal/mol and $\nu_o = (3.3 \pm 0.7) \times 10^{32}$ molecules/(cm^2 s).

The effects of the acid impurities on the D_2O desorption kinetics are associated with changes in the hydrogen bonding network and perturbed D_2O mobility in ice. For HNO_3-dosed D_2O ice multilayers, the decrease in the D_2O desorption rate is attributed to stable HNO_3-hydrate cage formation and reduced D_2O mobility in the ice lattice. In contrast, the increase in the D_2O desorption rate from HCl-dosed D_2O ice multilayers is assigned to Bjerrum L-defect formation, disruption of the hydrogen-bonding network and enhanced D_2O mobility in the ice lattice. The HNO_3 and HCl impurities are predicted to alter D_2O desorption rates significantly at stratospheric and upper tropospheric temperatures of 180−250 K. Assuming a unity sticking coefficient, the smaller D_2O desorption rates for ice with HNO_3 coverages ≥0.1 BL will lower the D_2O vapor pressure and enhance the stability of atmospheric ice particles. Conversely, the higher D_2O desorption rates for ice with HCl

coverages $\geq$0.1 BL will increase the D_2O vapor pressure and lower the stability of atmospheric ice particles. Alterations in the growth, formation, and stability of atmospheric ice crystals will subsequently affect heterogeneous atmospheric chemistry.

Acknowledgment. This work was supported by the National Science Foundation under Grant CHE-9528473.

References and Notes

(1) Molina, M. J.; Tso, T. L.; Molina, L. T.; Wang, F. C. Y. *Science* **1987**, *238*, 1253.
(2) Tolbert, M. A.; Rossi, M. J.; Malhotra, R.; Golden, D. M. *Science* **1987**, *238*, 1258.
(3) Solomon, S.; Garcia, R. R.; Rowland, F. S.; Wuebbles, D. J. *Nature* **1986**, *321*, 755.
(4) Turco, R. P.; Toon, O. B.; Hamill, P. *J. Geophys. Res.* **1989**, *94*, 16493.
(5) Hanson, D. R.; Ravishankara, A. R. *J. Geophys. Res.* **1991**, *96*, 5081.
(6) Kouchi, A. *J. Cryst. Growth* **1990**, *99*, 1220.
(7) Grim, R. J. A.; Greenberg, J. M. *Astr. Astrophys.* **1987**, *181*, 155.
(8) Mayer, E.; Pletzer, R. *Nature* **1986**, *319*, 298.
(9) Mukai, T. *Astr. Astrophys.* **1986**, *164*, 397.
(10) Klinger, K., Benest, D., Dollfus, A., Smoluchowski, R., Eds. *Ices in the Solar System*; Reidel: Dordrecht, 1985.
(11) Mendis, D. A.; Houpis, H. L. F.; Marconi, M. L. *Fundam. Cosmic Phys.* **1985**, *10*, 1.
(12) Delsemme, A. H. *Comets*; University of Arizona Press: Tucson, 1982; p 85.
(13) Solomon, S. *Rev. Geophys.* **1988**, *26*, 131.
(14) Tabazadeh, A.; Turco, R. P. *J. Geophys. Res.* **1993**, *98*, 12727.
(15) Toon, O. B.; Turco, R. P.; Westphal, D.; Malone, R.; Liu, M. S. *J. Atmos. Sci.* **1988**, *45*, 2123.
(16) See entire issue *Geophys. Res. Lett.* **1990**, *17*, 313.
(17) Leu, M.-T. *Geophys. Res. Lett.* **1988**, *15*, 851.
(18) Leu, M.-T. *Geophys. Res. Lett.* **1988**, *15*, 17.
(19) Borrmann, S.; Solomon, S.; Dye, J. E.; Luo, B. *Geophys. Res. Lett.* **1996**, *23*, 2133.
(20) Jensen, E. J.; Toon, O. B.; Selkirk, H. B.; Spinhirne, J. D.; Schoeberl, M. R. *J. Geophys. Res.* **1996**, *101*, 21361.
(21) Zondlo, M. A.; Barone, S. B.; Tolbert, M. A. *Geophys. Res. Lett.* **1997**, *24*, 1391.
(22) Abbatt, J. P. D. *Geophys. Res. Lett.* **1997**, *24*, 1479.
(23) Ramanathan, V.; Collins, W. *Nature* **1991**, *351*, 27.
(24) Stephens, G. L.; Tsay, S.-C.; Stackhouse, J., P. W.; Flatau, P. J. *J. Atmos. Sci.* **1990**, *47*, 1742.
(25) Ackerman, T. P.; Liou, K.-N.; Valero, F. P. J.; Pfister, L. *J. Atmos. Sci.* **1988**, *45*, 1606.
(26) Dye, J. E.; Baumgardner, D.; Gandrud, B. W.; Kawa, S. R.; Kelly, K. K.; Loewenstein, M.; Ferry, G. V.; Chan, K. R.; Gary, B. L. *J. Geophys. Res.* **1992**, *97*, 8015.
(27) Anderson, J. G.; Toon, O. B. *Geophys. Res. Lett.* **1993**, *20*, 2499.
(28) Ravishankara, A. R.; Hanson, D. R. *J. Geophys. Res.* **1996**, *101*, 3885.
(29) Hanson, D. R.; Ravishankara, A. R.; Solomon, S. *J. Geophys. Res.* **1994**, *99*, 3615.
(30) Hanson, D. R.; Ravishankara, A. R. *J. Phys. Chem.* **1994**, *98*, 5728.
(31) Gage, K. S.; McAfee, J. R.; Carter, D. A.; Ecklund, W. L.; Riddle, A. C.; Reid, G. C.; Balsley, B. B. *Science* **1991**, *254*, 1771.
(32) Danielsen, E. F. *J. Geophys. Res.* **1993**, *98*, 8665.
(33) Danielsen, E. F. *Geophys. Res. Lett.* **1982**, *9*, 605.
(34) Haynes, D. R.; Tro, N. J.; George, S. M. *J. Phys. Chem.* **1992**, *96*, 8502.
(35) Brown, D. E.; George, S. M.; Huang, C.; Wong, E. K. L.; Rider, K. B.; Smith, R. S.; Kay, B. D. *J. Phys. Chem.* **1996**, *100*, 4988.
(36) Brown, D. E.; George, S. M. *J. Phys. Chem.* **1996**, *100*, 15460.
(37) Livingston, F. E.; Whipple, G. C.; George, S. M. *J. Phys. Chem.* **1997**, *101*, 6127.
(38) Livingston, F. E.; Whipple, G. C.; George, S. M. *J. Chem. Phys.* **1998**, *108*, 2197.
(39) Livingston, F. E.; Smith, J. A.; George, S. M. *Surf. Sci.*, in press.
(40) Livingston, F. E.; George, S. M. *J. Phys. Chem. B* **1998**, submitted for publication.
(41) George, S. M.; Livingston, F. E. *Surf. Rev. Lett.* **1997**, *4*, 771.
(42) Sack, N. J.; Baragiola, R. A. *Phys. Rev. B: Condens. Matter* **1993**, *48*, 9973.
(43) Bryson, C. E., III; Cazcarra, V.; Levenson, L. L. J. *Chem. Eng. Data* **1974**, *19*, 107.
(44) Davy, J. G.; Somorjai, G. A. *J. Chem. Phys.* **1971**, *55*, 3624.
(45) Hinch, B. J.; Dubois, L. H. *J. Chem. Phys.* **1991**, *96*, 3262.
(46) Livingston, F. E.; Smith, J. A.; George, S. M. **1998**, manuscript in preparation.
(47) Koehler, B. G.; McNeill, L. S.; Middlebrook, A. M.; Tolbert, M. A. *J. Geophys. Res.* **1993**, *98*, 10563.
(48) Tolbert, M. A.; Middlebrook, A. M. *J. Geophys. Res.* **1990**, *95*, 22423.
(49) Diehl, K.; Mitra, S. K.; Pruppacher, H. R. *Atmos. Res.* **1998**, *47*−*48*, 235.
(50) Chen, J.-P.; Crutzen, P. J. *J. Geophys. Res.* **1994**, *99*, 18847.
(51) Nelson, J. T.; Baker, M. B. *J. Geophys. Res.* **1996**, *101*, 7033.
(52) Mak, C. H.; Brand, J. L.; Deckert, A. A.; George, S. M. *J. Chem. Phys.* **1986**, *85*, 1676.
(53) Deckert, A. A.; Brand, J. L.; Arena, M. V.; George, S. M. *Surf. Sci.* **1989**, *208*, 441.
(54) George, S. M.; DeSantolo, A. M.; Hall, R. B. *Surf. Sci.* **1985**, *159*, L425.
(55) Warren, S. G. *Appl. Opt.* **1984**, *23*, 1206.
(56) Brand, J. L.; George, S. M. *Surf. Sci.* **1986**, *167*, 341.
(57) *American Institute of Physics Handbook*, 3rd ed.: McGraw-Hill Book Co.: New York, 1982.
(58) LaPlaca, S.; Post, B. *Acta Crystallogr.* **1960**, *13*, 503.
(59) Hanson, D.; Mauersberger, K. *Geophys. Res. Lett.* **1988**, *15*, 855.
(60) Hanson, D. R. *Geophys. Res. Lett.* **1990**, *17*, 421.
(61) Worsnop, D. R.; Fox, L. E.; Zahniser, M. S.; Wofsy, S. C. *Science* **1993**, *259*, 71.
(62) Ritzhaupt, G.; Devlin, J. P. *J. Phys. Chem.* **1991**, *95*, 90.
(63) Smith, R. H.; Leu, M.-T.; Keyser, L. F. *J. Phys. Chem.* **1991**, *95*, 5924.
(64) Koehler, B. G.; Middlebrook, A. M.; Tolbert, M. A. *J. Geophys. Res.* **1992**, *97*, 8065.
(65) Middlebrook, A. M.; Koehler, B. G.; McNeill, L. S.; Tolbert, M. A. *Geophys. Res. Lett.* **1992**, *12*, 2417.
(66) Gilbert, A. S.; Sheppard, N. *J. Chem. Soc., Faraday Trans.* **1973**, *69*, 1628.
(67) Abbatt, J. P.; Beyer, K. D.; Fucaloro, A. F.; McMahon, J. R.; Woolridge, P. J.; Zhang, R.; Molina, M. J. *J. Geophys. Res.* **1992**, *97*, 15819.
(68) Graham, J. D.; Roberts, J. T. *J. Phys. Chem.* **1994**, *98*, 5974.
(69) Foster, K. L.; Tolbert, M. A.; George, S. M. *J. Phys. Chem.* **1997**, *101*, 4979.
(70) Vandoni, M. R. *Mem. Serv. Chim. Etat (Paris)* **1944**, *31*, 87.
(71) Grant, J. T.; Haas, T. W. *Surf. Sci.* **1970**, *21*, 76.
(72) Livingston, F. E.; George, S. M. *Defect and Diffusion Forum, Pt. A* **1998**, *160*−*161*, 25.
(73) Langmuir, I. *J. Phys. Chem.* **1929**, *31*, 1719.
(74) Eisner, H. S.; Quince, B. W.; Slack, C. *Discuss. Faraday Soc.* **1960**, *22*, 86.
(75) Derjaguin, B. V.; Fedoseyev, V. A.; Rosenweig, L. A. *J. Colloid Interface Sci.* **1966**, *22*, 45.
(76) Snead, C. C.; Zung, J. T. *J. Colloid Interface Sci.* **1968**, *27*, 25.
(77) Garrett, W. D. *J. Atmos. Sci.* **1971**, *28*, 816.
(78) Hobbs, P. V. *Ice Physics*; Clarendon Press: Oxford, 1974.
(79) Granicher, H. *Phys. Kondens. Mater.* **1963**, *1*, 1.
(80) Glen, J. W. *Sci. Prog., Oxf.* **1969**, *57*, 1.
(81) Jones, S. J. *Phys. Lett.* **1967**, *25A*, 366.
(82) Jones, S. J.; Glen, J. W. *Philos. Mag.* **1969**, *19*, 13.
(83) Young, I. G.; Salomon, R. E. *J. Chem. Phys.* **1968**, 48, 1635.
(84) Gertner, B. J.; Hynes, J. T. *Science* **1996**, *271*, 1563.
(85) Nakamura, T.; Jones, S. J. *Scr. Met.* **1970**, *4*, 123.
(86) Poshusta, R. D.; Tseng, D. C.; Hess, A. C.; McCarthy, M. I. *J. Phys. Chem.* **1993**, *97*, 7295.
(87) Delaplane, R. G.; Taesler, I.; Olovsson, I. *Acta Crystallogr.* **1975**, *B31*, 1486.
(88) Hanson, D. R.; Ravishankara, A. R. *J. Phys. Chem.* **1992**, *96*, 2682.
(89) Chu, L. T.; Leu, M.-T.; Keyser, L. F. *J. Phys. Chem.* **1993**, *97*, 7779.
(90) Delzeit, L.; Powell, K.; Uras, N.; Devlin, P. *J. Phys. Chem. B* **1997**, *101*, 2327.
(91) Peter, T.; Bruhl, C.; Crutzen, P. J. *Geophys. Res. Lett.* **1991**, *18*, 1465.
(92) Ramaswamy, V. *Geophys. Res. Lett.* **1988**, *15*, 863.
(93) Braham, R. R. *J. Atmos. Sci.* **1967**, *24*, 311.
(94) Braham, R. R.; Spyers-Duran, P. *J. Appl. Meterol.* **1967**, *6*, 1053.
(95) Biermann, U. M.; Crowley, J. N.; Huthwelker, T.; Moortgat, G. K.; Crutzen, P. J.; Peter, T. *Geophys. Res. Lett.* **1998**, submitted for publication.
(96) Schulze, F.-W.; Cammenga, H. K. *Ber. Bunsen-Ges. Phys. Chem.* **1980**, *84*, 163.
(97) Mills, A. F.; Seban, R. A. *Int. J. Heat Mass Transfer* **1967**, *10*, 1815.
(98) Tschudin, K. *Helv. Phys. Acta* **1946**, *19*, 91.
(99) Alty, T.; Mackay, C. A. *Proc. R. Soc. London* **1935**, *149*, 104.

(100) Kramers, H.; Stemerding, S. *Appl. Sci. Res. A* **1953**, *3*, 73.
(101) Warner, J. *J. Atmos. Sci*. **1969**, *26*, 1272.
(102) Sinarwalla, A. M.; Alofs, D. J.; Carstens, D. J. *J. Atmos. Sci.* **1975**, *32*, 592.
(103) Narusawa, M.; Springer, G. S. *J. Colloid Interface Sci.* **1975**, *50*, 392.
(104) Pruger, W. *Z. Phys.* **1940**, *115*, 202.
(105) Delaney, L. J.; Houston, R. W.; Eagleton, L. C. *Chem. Eng. Sci.* **1964**, *19*, 105.
(106) Heras, J. M.; Asensio, M. C.; Estiu, G.; Viscido, L. *Chem. Scr.* **1984**, *23*, 245.
(107) Marti, J.; Mauersberger, K. *Geophys. Res. Lett.* **1993**, *20*, 363.
(108) Jancso, G.; Pupezin, J.; Alexander Van Hook, W. *J. Phys. Chem.* **1970**, *74*, 2984.